The substitution of Mn by Ni in $(Mn,Fe)_2(P,Si)$ compounds and its magnetocaloric consequences.

A comparison with research studies on cobalt regarding tuneable curie temperature, hysteresis and magnetization.

By

Levi Pieter

in partial fulfilment of the requirements for the degree of

Bachelor of Science
in Applied Physics

at the Delft University of Technology,

Supervisors:	Prof. dr. E.H. Brück
	Dr. N.H. Van Dijk
Tutor:	A. Kiecana
Student number:	4373448
Date:	27/03/2020

TU Delft

Abstract

With green energy well on its way to becoming a necessity rather than a commodity it is vital to not only focus on improving the source of energy, but also the efficiency of the eventual energy usage.
Vapor-compression based household refrigerators are one of the most used electrical appliances in the common household and consume electricity throughout the day, so finding a more efficient alternative would be beneficial. One such alternative uses the magnetocaloric effect as cooling mechanism and could theoretically reach a much higher efficiency. However, the search for the right material with the right characteristics for the commercial realization of this technology is still ongoing and this thesis aims to assist in making progress in said search.
The focus of this thesis is on the substitution of manganese with nickel in Mn-Fe-P-Si compounds and how the magnetocaloric properties of these compounds hold up against similar compounds that had manganese substituted with cobalt as this lowered the Curie temperature and decreased the thermal hysteresis, which are favourable results. Unfortunately, there are a few factors such as price and criticality that motivated replacing cobalt with a close relative such as nickel in hope of achieving similar results.
Measurements done with a superconducting quantum interference device (SQUID) indicated that the synthesized Mn-Fe-Ni-P-Si compounds have very similar magnetic properties to the Mn-Fe-Co-P-Si compounds. Differential scanning calorimetry (DSC) measurements showed that both compounds reduce thermal hysteresis similarly, but the nickel compounds are capable of lowering the curie temperature much more with increased doping compared to the cobalt compounds. X-ray powder diffraction (XRD) analysis proved that nickel is substituted in the proper place and that the decreasing Curie temperature is the result of a change in the ratio of the unit cell parameters *a* and *c*.

Nickel thus showed to be an excellent replacement of cobalt to be used to substitute manganese with to lower the Curie temperature of the initial Mn-Fe-P-Si compound and reduce thermal hysteresis.
More research could be done on further tuning the composition by for example increasing the silicon doping as this has shown to increase the Curie temperature rather than decrease it whilst also reducing the thermal hysteresis. Combined with the results from this thesis it could lead to a composition with more favourable magnetocaloric characteristics.

Contents

1 Introduction

The recent worldwide growth of interest concerning the topic of global warming in the wake of the UN Global Climate Action Summit of 2019 has stimulated the search for greener energy sources and further increasing the efficiency and environmental friendliness of our current appliances.
One such appliance that is widely used in both the domestic and public sector is the conventional refrigerator. It is safe to say that roughly every household has at least one refrigerator and with such an abundance of use comes the obligation for optimization. This is where the technology involving the magnetocaloric effect comes into play. A refrigerator operating through the magnetocaloric effect with the use of an alloy based on gadolinium has shown to have an efficiency of 60% of the theoretical limit [1, 2]. A vast improvement from the traditional vapour-compression refrigerator, which could thus far only reach about 45% of that same limit [3]. Along with an improvement in cooling efficiency comes the fact that this technique omits the use of polluting refrigerants such as the commonly used hydrofluorocarbons (HFCs) which contribute to global warming [4].

1.1 The Magnetocaloric effect.

The magnetocaloric effect (often abbreviated as MCE) is one of the consequences of the link between electromagnetism and thermodynamics. In principle it describes the change in temperature of a magnetic material as a result of the presence of an external magnetic field due to a change in the magnetic entropy ΔS_B. It was first properly discovered and examined by Pierre Weiss and Auguste Piccard in 1917 [5, 6]. Its first use as cooling mechanism was proposed independently by Debye in 1926 and Giauque in 1927 under the practical term *adiabatic demagnetization* [7, 8].

1.2 Magnetic refrigeration.

Giauque went on together with MacDougall to build a setup that could obtain a temperature of 0.53 ºK from a starting temperature of 3.4 ºK through the use of the magnetocaloric effect of gadolinium in 1933 [9] giving scientists a way to reach temperatures closer to the absolute zero than ever before. It was not until 1976, however that a scientist by the name of G.V. Brown managed to create a device that had an operational temperature span from -1 ºC to 46 ºC once again using gadolinium and a magnetic field of 7 T [10].

1.3 Magnetocaloric compounds.

With pure gadolinium as the pioneer when it comes to suitable magnetocaloric materials that operate under room-temperature, the search for better candidates began. Unfortunately, there are many expectations which the material must live up to if it is going to be integrated in the commercial market. It must be non-toxic, relatively cheap, abundant in the Earth's crust and, for it to be a candidate at all, it must also display a large magnetocaloric effect around room-temperature under the influence of a magnetic field smaller than 1 T. The reasoning behind the last condition being that the use of permanent magnets is desired since they do not require electricity to generate a magnetic field, meaning that their implementation can be expected to lower the refrigerator's efficiency less than the use of electromagnets.

A comparison of several magnetocaloric materials that have been tested over the years is displayed in the following table.

Table 1. A comparison of different magnetocaloric materials potentially viable for magnetocaloric refrigeration [11].

Material	T range K	$\Delta S_{B,max}$ (2T) J kg^{-1} K^{-1}	ΔT (2T) K	Tc K	Costs €/kg (2005)	Density 10^3 kg m^{-3}
Gd	270-310	5	5.8	293	20	7.9
$Gd_5Ge_2Si_2$	150-290	27	6.6	272	60	7.5
La(Fe,Si)H	180-320	19	7	300	8	7.1
MnAs	220-320	32	4.1	287	10	6.8
MnNiGa	310-350	15	2	317	10	8.2
MnFe(P,As)	150-450	32	6	292	7	7.3

The important numerical properties that are sought after are:

- A high maximum change in magnetic entropy ($\Delta S_{B,max}$) to facilitate a high magnetocaloric effect
- A high adiabatic temperature change (ΔT)
- A low thermal hysteresis (ΔT_{hys}) so that the refrigerator does not have to cool or heat excessively to cross the Curie temperature point.
- A Curie temperature (Tc) around room temperature to ensure that the refrigerator works best in a standard indoor environment.
- A relatively low cost

As can be derived from the table, an alloy of manganese, iron and phosphor has a large thermal range with a relatively high entropy change whilst being relatively cheap compared to the other contenders. However, adding cobalt to this alloy has proven to lower both the Curie temperature and the width of the thermal hysteresis (ΔT_{hys}). However, cobalt is more than twice as expensive as nickel with cobalt being valued at around $30 per kilogram and nickel, its neighbor on the periodic table, at around $12 per kilogram at the time of writing [12, 13]. Aside from the price, cobalt is also highly demanded critical resource for its use in lithium-ion batteries, the demand for which is increasing with the growing number of electric vehicles in use, and around 55% of the cobalt used comes from the politically unstable Democratic Republic of Congo which affects the certainty of supply and introduces political and ethical factors to the use of cobalt [14].

1.4 Thesis outline

This bachelor thesis will contain the research on how the substitution of manganese by nickel affects the magnetocaloric properties of the compound. These properties are evaluated by measuring and calculating the Curie temperature Tc, the latent heat, the order of the magnetic phase transition, the effect of and presence of impurity phases and the magnetization as a function of the temperature. These results will then be compared to reference compounds of Mn-Fe-Co-P-Si and the initial compound of Mn-Fe-P-Si.
The second chapter will provide the necessary thermodynamic background theory for the magnetocaloric effect and the experimental methods utilized can be found in the third chapter. The fourth chapter will contain the results of the measurements and calculations with their necessary explanation after which the fifth and final chapter will contain what can be concluded from this research.

2 Theory

This chapter serves to explain the physics and thermodynamics behind the magnetocaloric effect and how some results from the measurements are transformed to output desired variables.

2.1 Gibbs free energy

For the evaluation of a material its magnetothermal effects in an externally applied magnetic field *B*, at a temperature *T* and under a pressure *p* it is useful to look at the Gibbs free energy *G*:

$$G = U - TS + pV - MB \tag{1}$$

With *U* as the internal energy, *S* the entropy, *V* the volume, *M* the magnetization. Its differential *dG* is calculated by differentiating *G* and substituting *U* according to the first law of thermodynamics resulting in*:*

$$dG = Vdp - SdT - MdB \tag{2}$$

Taking the partial derivatives of this function will result in the following expressions:

$$V(T,B,p) = \left(\frac{\partial G}{\partial p}\right)_{T,B} \tag{3}$$

$$S(T,B,p) = -\left(\frac{\partial G}{\partial T}\right)_{B,p} \tag{4}$$

$$M(T,B,p) = -\left(\frac{\partial G}{\partial B}\right)_{T,p} \tag{5}$$

Applying Schwarz' theorem, which is defined as:

$$\frac{\partial}{\partial x_j}\left(\frac{\partial \phi}{\partial x_i}\right) = \frac{\partial}{\partial x_i}\left(\frac{\partial \phi}{\partial x_j}\right) \tag{6}$$

to equations 4 and 5 and differentiate with respect to the magnetic field *B* and the temperature *T* we obtain the following so-called Maxwell relation:

$$\left(\frac{\partial S}{\partial B}\right)_{T,p} = \left(\frac{\partial M}{\partial T}\right)_{B,p} \tag{7}$$

2.2 Change in magnetic entropy (ΔS_B) and the specific heat capacity ($C_{p,B}$)

As mentioned before, the change in magnetic entropy (ΔS_B) is what eventually results in the change in temperature of the material so therefore it is an important quantity. It can be calculated by first taking the differential of the total entropy in the system expressed in terms of the magnetic field (*B)*, the temperature (*T),* and the pressure (*p)*:

$$dS(T,B,p) = \left(\frac{\partial S}{\partial T}\right)_{B,p} dT + \left(\frac{\partial S}{\partial B}\right)_{T,p} dB + \left(\frac{\partial S}{\partial p}\right)_{T,B} dp \tag{8}$$

Taking into account that the change in entropy that we're interested in is a result of a changing magnetic field in isobaric (dp = 0) and isothermal (dT = 0) conditions and combining this with the Maxwell relation from equation 7, we can simplify equation 8 to:

$$dS(T,B,p) = \left(\frac{\partial M}{\partial T}\right)_{B,p} \tag{9}$$

Which can then be integrated to form an expression for *S*:

$$S(T,B,p) = \int_{B_1}^{B_2} \left(\frac{\partial M}{\partial T}\right)_{B,p} dB \tag{10}$$

If we then consider the general formula for the specific heat capacity and the second law of thermodynamics for a reversible process in a closed system, respectively:

$$C_* = \left(\frac{\delta Q}{T}\right)_* \tag{11}$$

$$dS = \frac{\delta Q}{dT} \tag{12}$$

with (*) indicating the variables that remain constant, which in this case are the external magnetic field (*B*) and the pressure (*p*), we can combine equations 11 and 12 to obtain the following expression:

$$C_{p,B}(T,B) = T\left(\frac{\partial S}{\partial T}\right)_{B,p} \tag{13}$$

Which can be substituted in equation 8 and under constant pressure and magnetic field results in:

$$dS(T,B,p) = \frac{C_{p.B}(T,B)}{T} \tag{14}$$

Further combining equations 9, 10 and 14 will lead to the integral:

$$S(T,B,p) = S_0 + \int_0^T \left(\frac{C_{p.B}(T',B)}{T'}\right)_{B,p} dT' \tag{15}$$

The last step to reach an expression for the change in magnetic entropy is to reintroduce the change in magnetic field from equation 10:

$$\Delta S_B(T,\Delta B) = \int_0^T \left(\frac{C_{p.B}(T',B_2) - C_{p.B}(T',B_1)}{T'}\right)_p dT' \tag{16}$$

2.3 Adiabatic temperature change (ΔT_{ad})

Now considering equation 8 not only under constant pressure but also under adiabatic conditions (meaning both *dS* and *dp* are nullified*)* in combination with equations 7 and 13 will deliver the differential of the temperature as result of, amongst others, a change in magnetic field:

$$dT = -\frac{T}{C_{p,B}}\left(\frac{\partial M}{\partial T}\right)_{p,B} dB \tag{17}$$

Integration with respect to the magnetic field and its change from B_1 to B_2 guides us directly to the formula for the adiabatic temperature change:

$$\Delta T_{ad}(T, \Delta B, p) = -\int_{B_1}^{B_2} \frac{T}{C_{p,B}}\left(\frac{\partial M}{\partial T}\right)_{p,B} dB \tag{18}$$

From this equation it can be easily deduced that the temperature change as a result of the magnetocaloric effect increases as $\left(\frac{\partial M}{\partial T}\right)_{p,B}$ increases.

2.4 Magnetic phase transition and Curie temperature

As a ferromagnetic material gets heated up past its Curie temperature (*Tc*) it will undergo a phase transition and become paramagnetic. This process can be reversible, which is shown when the material cools down and crosses the Curie temperature again to become ferromagnetic once more. However, this *Tc* is usually offset depending on whether it was reached through heating or cooling by a ΔT_{hys} and thus displays a form of thermal hysteresis.
Furthermore, this phase transition can be characterized as being either a First-Order Magnetic phase Transition (FOMT) or a Second-Order Magnetic phase Transition (SOMT) relating respectively to whether or not the transitions are discontinuous or continuous in the first derivative of the Gibbs free energy, especially equation 4. A visual representation of these phase transitions can be seen in figure 1.

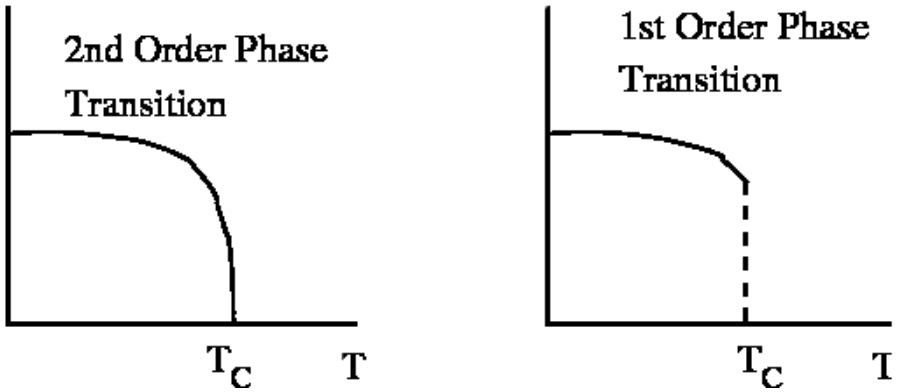

Figure 1: A figure displaying the difference in continuity between a 1st order phase transition and a 2nd order phase transition.

As can be concluded from equation 18, maximizing ΔT_{ad} can be achieved by maximizing $\frac{\partial M}{\partial T}$, thus by steepening the slope of the phase transition and minimizing the width of the hysteresis ΔT_{hys}. However, the slope is the steepest in a FOMT while the hysteresis width is the smallest in a SOMT. This means that the ideal case is somewhere in between a FOMT and a SOMT.

3 Experimental Techniques

For this research 8 new samples were made that adhere to the formula $Mn_{0.62-x}Fe_{1.33}Ni_xP_{0.66}Si_{0.34}$ starting with x = 0.01 and x = 0.02 after which x increases with steps of 0.02 for each subsequent sample until a final value of x = 0.14. These samples were given the names LP01-LP08.

Similar samples containing cobalt instead of nickel had already been prepared and measured by A. Kiecana (FAME, TU Delft). This thesis will include some discussion of these samples and results as well for comparative purposes.

3.1 Sample preparation

The first step to preparing the samples is creating the correct mixtures of manganese (99.7% pure), iron (99% pure), nickel (99.9% pure), iron phosphide (99.5% pure) and silicon (99.7% pure) powder with the assistance of a Mettler Toledo XS105 DualRange which has a readability from 0.1 to 0.01 mg.

3.1.1 Mechanical alloying

The next step is to create alloys from these mixtures. The alloys mentioned in this thesis were initially created through a process called mechanical alloying, specifically by using a Fritsch GmbH Pulverisette planetary ball mill. The mixtures were individually loaded into tungsten-carbide jars (80 ml) which already contained 7 tungsten-carbide balls (10 mm in diameter). The jars were then brought into an argon atmosphere and vacuum sealed before being secured on a rotating plate in the machine.
The planetary ball mill owes its name to the planet-like fashion in which the jars move, since they do not only rotate on the rotating plate, but also spin around their own axis. At high speeds the balls inside the jars repeatedly collide with its walls and grind the mixture as it is caught in between [15]. This eventually creates an extremely fine powder consisting of the desired alloy. A schematic displaying the concept of the balls' motion inside the jars is shown in figure 2. The samples used in this thesis were ball milled for 10 hours at 350 rounds per minute.

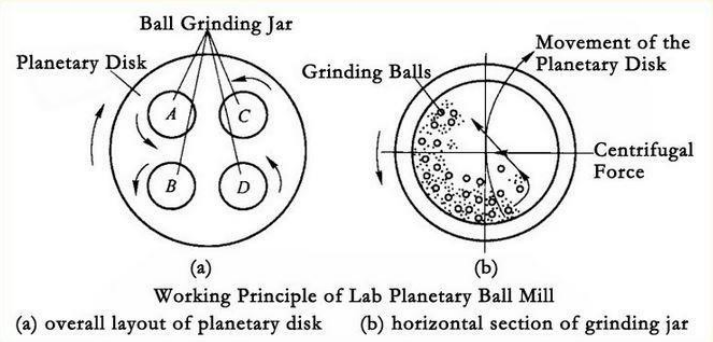

Figure 2: Schematic displaying the concept behind a planetary ball mill [16].

3.1.2 Annealing

After the ball milling process the resulting fine alloy powder is pressed into tablets, which are subsequently sealed into separate quartz tubes filled with argon gas. These tubes were placed inside an annealing furnace at a temperature of 1100 ºC and quenched after being annealed for 20 hours.
This form of heat treatment at the aforementioned temperature has shown to reduce magnetic hysteresis and counteract the formation of impurity phases to a certain degree [17].
After the annealing process the samples are directly quenched in a vat containing water at room temperature.

3.1.3 Overcoming the virgin effect

When a $(Mn,Fe)_2(P,Si)$ compound, such as was synthesized in the previous steps, undergoes a magnetic phase transition for the first time it will do so at a lower temperature than any subsequent magnetic phase transitions. This so-called “virgin effect” arises from a metastable state embedded into the sample as a result of the annealing process and has shown to stabilize permanently after the sample’s first magnetic phase transition through cooling. Since the virgin effect attributes to an initially lower Curie temperature it was decided to cool the samples in liquid nitrogen, since this has proven to eradicate the virgin effect effectively preventing this phenomenon from affecting the measurement results [18, 19].

Lastly the samples were manually pulverized using a mortar and pestle and could finally be introduced to the various measuring apparatus that were employed.

3.2 Measuring techniques

3.2.1 Differential Scanning Calorimetry (DSC)

Differential scanning calorimetry (DSC) is a measurement technique that evaluates the heat flux required to keep a sample at the same temperature as a reference sample under a steadily changing temperature [20]. This is useful for detecting the critical temperatures at which a material undergoes a magnetic phase transition as these transitions are accompanied by latent heat [21]. This means that if the sample of interest undergoes a phase transition whilst the reference sample does not, a higher or lower heat flux is required to keep the sample of interest at the same temperature as the reference sample depending on whether the phase transition is endothermic or exothermic. The DSC results included in this research were obtained using a DSC Q2000 manufactured by TA instruments. The device was set to perform two full cycles from 223 K to 323 K and back at a sweep rate of 10.00 K/min and the results were used to discover the Curie temperature, latent heat and the thermal hysteresis of each sample. An amount between 30 and 50 milligrams of each sample was sealed in a special Tzero® Aluminum pan also manufactured by TA Instruments to ensure the highest resolution and sensitivity during the measurements. A picture of a DSC sample stage accompanied by a schematic can be seen in figure 3.

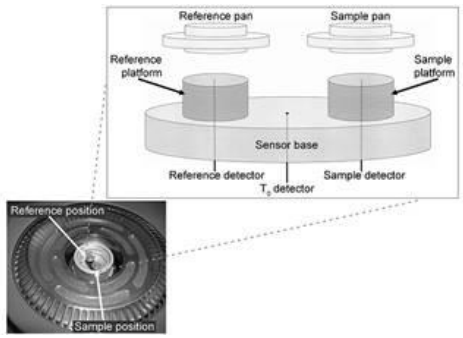

Figure 3: A picture of a DSC sample stage with a schematic.[22]

3.2.2 Superconducting Quantum Interference Device (SQUID)

The Quantum Design MPMS-5S and MPMS-XL SQUID's are extremely sensitive magnetometers that were utilized in this research to determine the magnetization of the samples as a function of an applied magnetic field while held at a constant temperature and subsequently to measure the magnetization as a function of the temperature while under the influence of a constant magnetic field.

The principle of the MPMS SQUIDs is that it contains a set of superconducting coils which pick up the electric current created when the magnetic sample moves through them as this gives rise to a change in magnetic flux [23].

The sequence measuring the magnetization as a function of the applied magnetic field would do so while increasing the magnetic field strength from 0 T to 5 T whilst keeping the temperature around 5 K and the two sequences measuring the magnetization as a function of the temperature did so while under the influence of a magnetic field strength of respectively 0.01 T and 1 T. At the same time the temperature during these two sequences would sweep from 5 K to 370 K at a rate of 2 K/min.

The choices regarding the temperature range and the various magnetic field strengths were all in accordance with the aim of this research to evaluate the magnetocaloric properties of the synthesized compounds for use in commercial magnetocaloric-based cooling devices designed to operate around room temperature and in low magnetic fields.

3.2.3 X-ray Powder Diffraction (XRD)

X-ray powder diffraction measurements were carried out to determine which impurity phases were present in the synthesized samples, how much of the sample they occupy in percentages and to acquire the lattice parameters of the crystal structure.
The x-ray powder diffraction measuring method depends on the elastic scattering of the x-rays off of the atoms in the crystal lattice and constructively interfering in a set direction at an angle θ bound by the spacing between the atomic layers d_{hkl} and the wavelength λ. An illustration of this process is shown in figure 4.

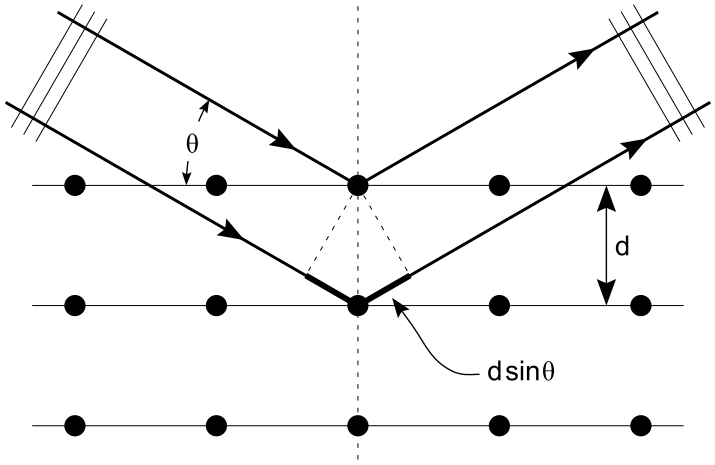

Figure 4: An illustration of x-rays scattering off of atoms in the crystal lattice [24].

These variables are connected through Bragg's Law which is defined as:

$$n\lambda = 2d_{hkl}\sin\,\theta \tag{19}$$

Allowing one to resolve the interatomic spacing with a known wavelength and scattering angle, which are respectively a property and the output of a diffractometer [25].

The diffractometer that was utilized for this research was a PANalytical X-pert Pro diffractometer that employed Cu K-alpha radiation and was equipped with an Anton Paar 450TTK Low-Temperature Chamber and a multichannel X'celerator detector. The diffraction patterns that were obtained as a result were refined using the Rietveld refinement method included in the FullProf Suite.

4 Results and discussion

4.1 DSC results

The DSC measurements showed that the Curie temperature of the samples containing nickel can be tuned downwards effectively by increasing the amount of nickel in the sample. This is in contrast with the samples containing cobalt, which displayed this effect for only small amounts of cobalt and this side-effect appears to stagnate quite quickly as is apparent in figure 5.

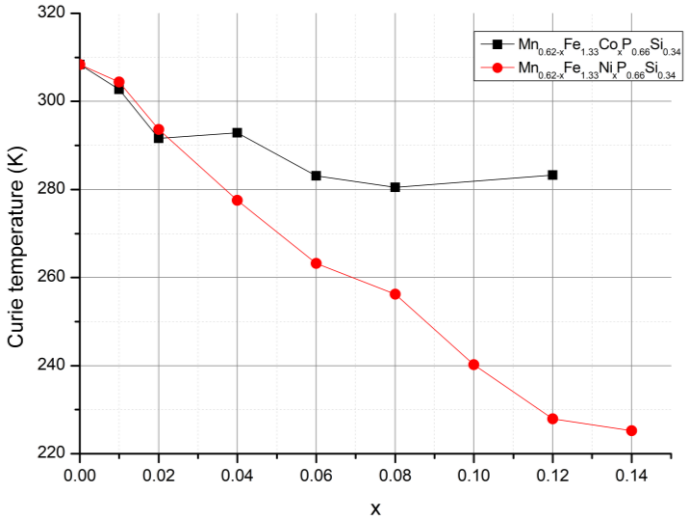

Figure 5: A plot displaying the decrease in Curie temperature for the samples containing cobalt and the samples containing nickel as a function of the amount of by which they were doped.

The difference between both sample sets with respect to their latent heat turned out to be only minimal, as shown in figure 6, which supports the notion that both compositions convert the order of their magnetic transition around similar composition percentages for both nickel and cobalt, namely between x = 0.04 (LP04) and x = 0.06 (LP05).

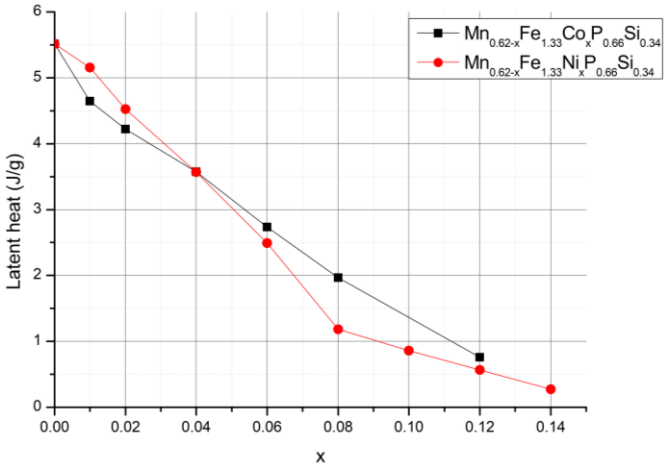

Figure 6: A plot which compares the latent heat present in $Mn_{0.62-x}Fe_{1.33}Ni_xP_{0.66}Si_{0.34}$ and in $Mn_{0.62-x}Fe_{1.33}Co_xP_{0.66}Si_{0.34}$ during their phase transition.

The DSC also measured the heat capacity of the samples as a function of temperature resulting in the graphs displayed in figure 7.

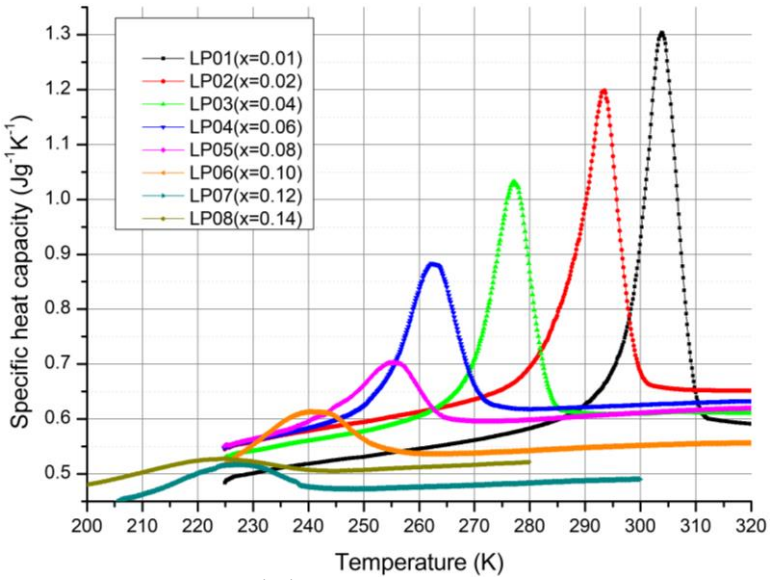

Figure 7: A graph displaying the specific heat capacity in $Jg^{-1}K^{-1}$ as a function of the temperature in Kelvin for each of the samples containing nickel during heating.

A trend is observed with the peak of the specific heat capacity starting off high and narrow and gradually becoming lower and wider as the amount of nickel doping increases indicating the progressive conversion of the magnetic phase transition from first-order to second-order [26]. .

4.2 SQUID results

The SQUID results confirmed that the magnetic phase transition changes order after LP04(x=0.06) as the hysteresis becomes exceedingly small for compositions with increased nickel doping as seen in figure 8.

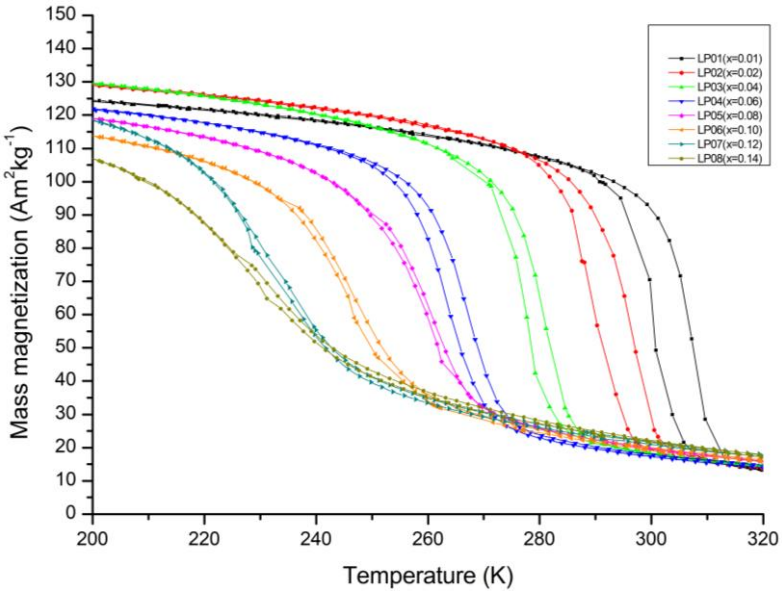

Figure 8: A graph illustrating the relation between the mass magnetization and the temperature of each of the samples containing nickel.

Manually calculating the maximum value of the negative derivative of each of these curves resulted in rough *dM/dT* values per sample. These values have been plotted in figure 9 together with those of the samples doped with cobalt.

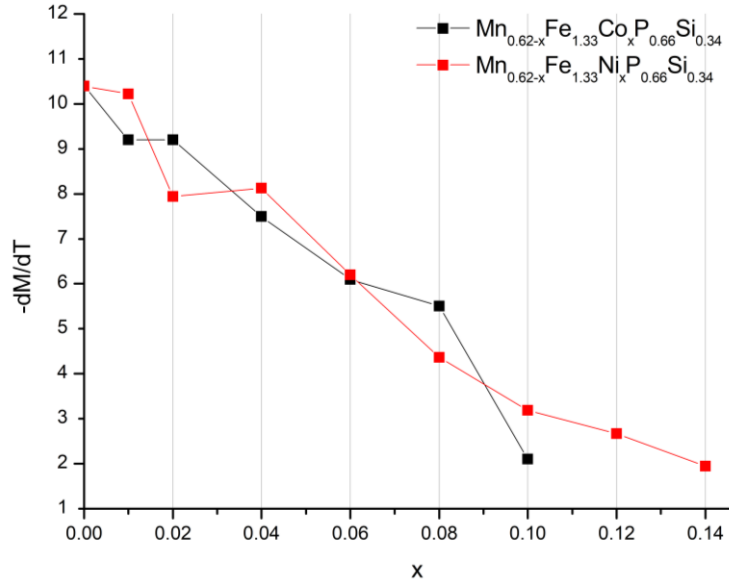

Figure 9: A plot which compares the maximum -*dM/dT* during heating as a function of *x* in $Mn_{0.62-x}Fe_{1.33}Ni_xP_{0.66}Si_{0.34}$ and in $Mn_{0.62-x}Fe_{1.33}Co_xP_{0.66}Si_{0.34}$

The *dM/dT* values of the samples containing cobalt appear to decrease at a slightly faster rate and confirming this statement would require more measurements. However, it is safe to say that the *dM/dT* values of Mn-Fe-P-Si compositions doped with nickel or cobalt are very similar.

Lastly the magnetization of the samples was measured as a function of the applied magnetic field. Plotting these values against the reciprocal value of the corresponding applied magnetic field gave a set of graphs that are shown in figure 10 along with their corresponding fit and the saturation magnetization values obtained by calculating the y-intercept of said fit.

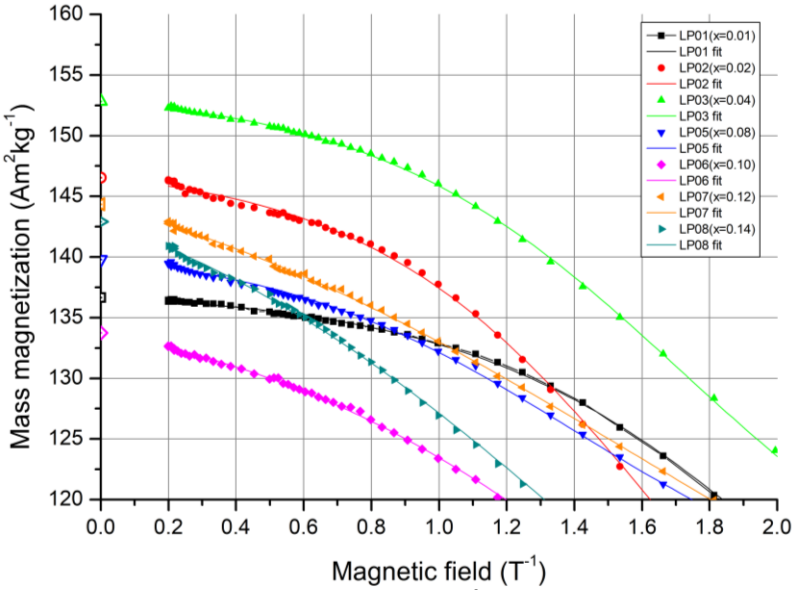

Figure 10: A graph displaying the relation between the mass magnetization (Am^2/kg) and the reciprocal of the magnetic field (1/T) for each of the samples containing nickel. A Boltzmann sigmoid curve was fitted through the data and the y-intercepts of these fitted curves are displayed on the y-axis.

The formula chosen for the fit corresponds to a Boltzmann sigmoid curve as the data formed a similar sigmoid-like shape that reaches a constant value in the limit of an infinite magnetic field while also approaching a constant in the limit of an absent magnetic field. More details surrounding this fit including the errors and calculated variables can be found in appendix A.

The extrapolated saturation values for the magnetization can be seen in figure 11 where they are plotted as a function of the amount of nickel doping.

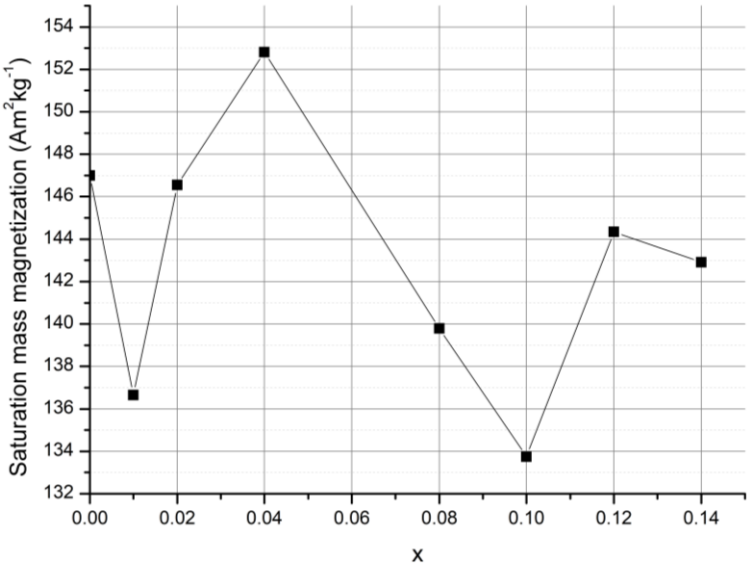

Figure 11: A graph plotting the extrapolated saturation values for the magnetization as a function of the amount of nickel doping in the compounds.

What is most noticeable is the rapid increase in saturation magnetization for $x = 0.04$ and the sharp decline in the saturation magnetization that can be seen for $x = 0.08$ and $x = 0.10$ referring to LP03, LP05 and LP06 respectively. This will be further discussed in the next chapter as it requires information gathered during the XRD measurements.

4.3 XRD Results

The XRD measurements were refined using Rietveld refinement with Fullprof. The results of these refinements are shown stacked in figure 12.

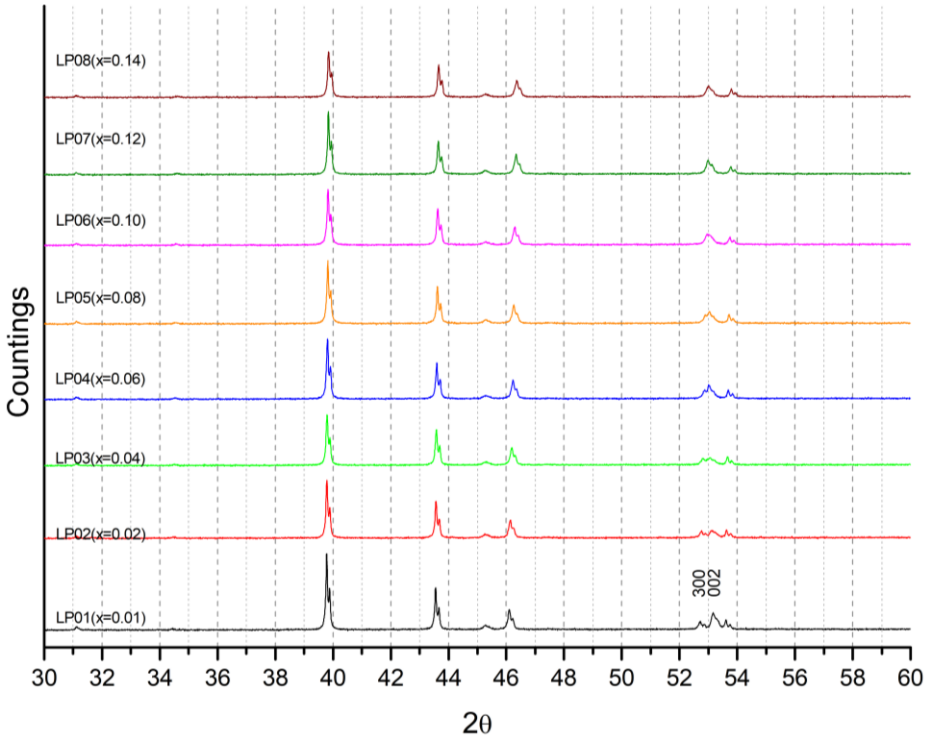

Figure 12: A stacked plot of the intensity as a function of 2Θ resulting from the refinement for all the samples containing nickel

The plots in figure 12 look almost identical except for the fact that the peaks corresponding with miller indices (300) and (002) appear to move towards each other and eventually merge as the nickel doping in the samples is increased. This indicates that the lattice parameters *a* and *c* are varying inversely, which was confirmed by the results of the Rietveld refinement [27].
An example of the results of one such refinement can be seen in figure 13 where the results for LP04 (x=0.06) are displayed and a full table containing all the variables resultant of the refinements including those of the cobalt samples can be found in appendix B.

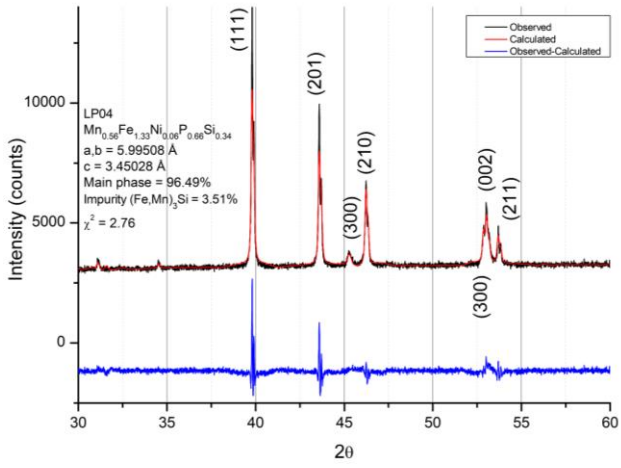

Figure 13: A plot displaying the Rietveld refinement results of LP04(x=0.06) including the miller indices, lattice parameters (Å), percentages of the various phases present and the χ^2 value.

The refinement results attributed a low and near constant percentage of the $(Fe,Mn)_3Si$ impurity phase to each of the $Mn_{0.62-x}Fe_{1.33}Ni_xP_{0.66}Si_{0.34}$ samples and a near negligible amount of the $(Fe,Mn)_5Si_3$ impurity phase as shown in figure 14.

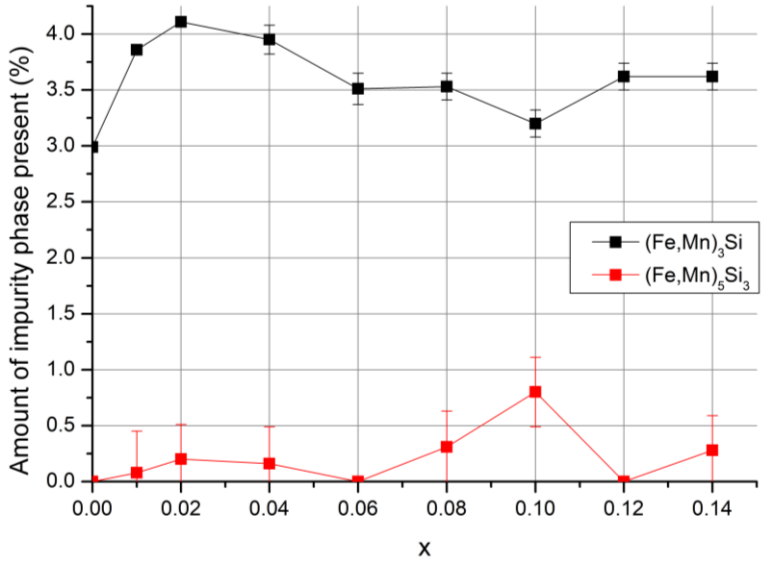

Figure 14: A graph displaying the percentage of impurity phase present in the samples containing nickel with added error bars.

Recalling the steep decline in saturation magnetization from figure 11 in the previous chapter for $x = 0.08$ and $x = 0.10$ it now seems that this drop in magnetization corresponds with a higher amount of $(Fe,Mn)_5Si_3$ phase present in the compound.

Furthermore, the refinement allowed for the extraction of the lattice parameters of the compounds, which were plotted as a ratio together in figure 15 with the Tc values obtained with the SQUID during the heating cycle. The plot not only displays the relation between the ratio of the lattice parameters (*c/a)* and *Tc,* but also its near linear relation with respect to the percentage of nickel doping *x*.

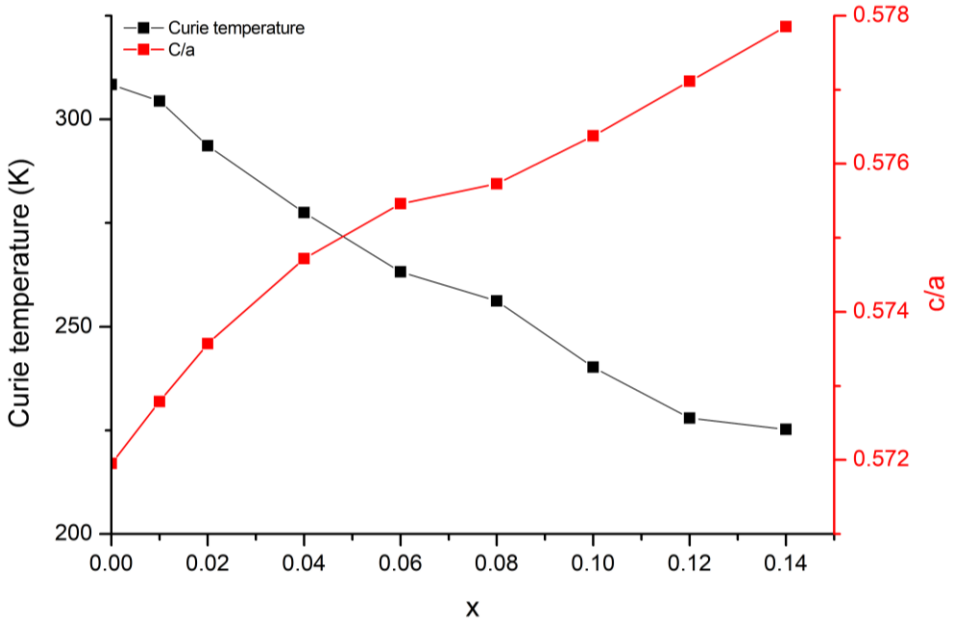

Figure 15: A plot showing how the c/a and Tc values of the nickel doped compounds depend on x as well as their interdependence.

Lastly the volume of the unit cell was evaluated as a function of *x* and plotted, which led to the graph displayed in figure 16.

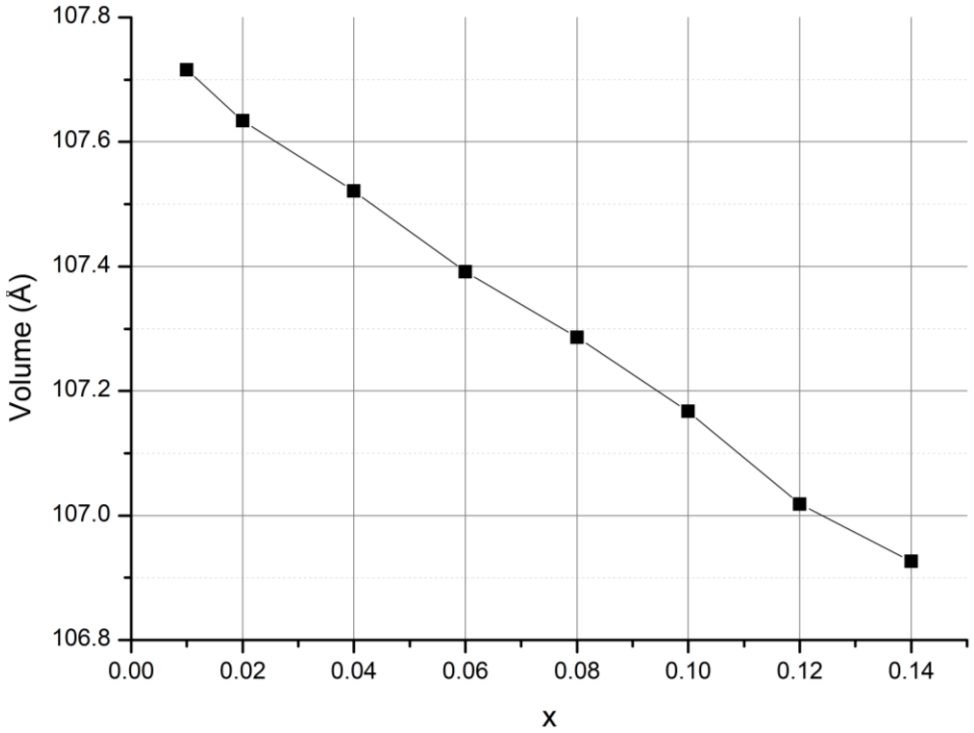

Figure 16: A plot displaying the unit cell volume (Å) as a function of x in $Mn_{0.62-x}Fe_{1.33}Ni_xP_{0.66}Si_{0.34}$.

The linear decrease of the unit cell volume indicates that manganese is indeed being replaced by nickel since nickel has a lower atomic radius than manganese and interstitial doping would be expected to cause an increase in unit cell volume rather than a decrease.

5 Conclusion

The substitution of manganese with nickel in $Mn_{0.62}Fe_{1.33}P_{0.66}Si_{0.34}$ compounds has shown to effectively decrease the Curie temperature more so than when manganese is substituted with cobalt in similar compounds, while other important characteristics such as *-dM/dT* and the order of magnetic phase transition, evaluated through the presence of latent heat, are very similar to compounds obtained through the substitution of manganese with cobalt.
The saturation magnetization of the prepared nickel compounds appears to be influenced by the amount of $(Fe,Mn)_5Si_3$ impurity phase present.

All in all it appears that nickel is a very good alternative for cobalt when it comes to tuning the curie temperature in Mn-Fe-P-Si compounds for applied magnetocaloric purposes such as the realization of magnetic refrigeration as it delivers similar results while being cheaper, less critical and more ethical alternative.

Further research could be done on tuning the other magnetocaloric properties of the compound to fit the requirements of magnetocaloric cooling technology. For example, substituting phosphorous with additional silicon has proven to increase the Curie temperature and decrease the magnetic hysteresis in similar compounds containing cobalt. Combining these two substitutions would perhaps lead to a compound with more favorable magnetocaloric properties.

References

[1] A.J. C. Zimm, A. Sternberg, V. Percharsky, K. Geschneidner Jr., M. Osborne, I. Anderson, *Description and Performance of a Near-Room Temperature Magnetic Refrigerator* in: Advances in Cryogenic Engineering Vol. 43, 1998, pp. 1759-1766.

[2] J. Lyubina, *Magnetocaloric materials for energy efficient cooling*, Journal of Physics D: Applied Physics, 50 (2017).

[3] O. Gutfleisch, M.A. Willard, E. Bruck, C.H. Chen, S.G. Sankar, J.P. Liu, *Magnetic materials and devices for the 21st century: stronger, lighter, and more energy efficient*, Adv Mater, 23 (2011) 821-842.

[4] G. Venkatarathnam, S. Srinivasa Murthy, *Refrigerants for vapour compression refrigeration systems*, Resonance, 17 (2012) 139-162.

[5] P. Weiss, A. Piccard, *Le phénomène magnétocalorique*, Journal de Physique Théorique et Appliquée, 7 (1917) 103-109.

[6] A. Smith, *Who discovered the magnetocaloric effect?*, The European Physical Journal H, 38 (2013) 507-517.

[7] P. Debye, *Einige Bemerkungen zur Magnetisierung bei tiefer Temperatur*, Annalen der Physik, 386 (1926) 1154-1160.

[8] W.F. Giauque, *A thermodynamic treatment of certain magnetic effects. A proposed method of producing temperatures considerably below 1° absolute*, Journal of the American Chemical Society, 49 (1927) 1864-1870.

[9] W.F. Giauque, D.P. MacDougall, *Attainment of Temperatures Below 1° Absolute by Demagnetization of $Gd_2(SO_4)_3 \cdot 8H_2O$*, Physical Review, 43 (1933) 768-768.

[10] G.V. Brown, *Magnetic heat pumping near room temperature*, Journal of Applied Physics, 47 (1976) 3673-3680.

[11] E. Brück, *Developments in magnetocaloric refrigeration*, Journal of Physics D: Applied Physics, 38 (2005) R381-R391.

[12] Trading Economics, *Cobalt*, 2020.

[13] Trading Economics, *Nickel*, 2020.

[14] D.B. P. Alves Dias, C. Pavel, N. Arvanitidis, *Cobalt: demand-supply balances in the transition to electric mobility*, in, Publications Office of the European Union, 2018.

[15] C. Suryanarayana, *Mechanical alloying and milling*, Progress in Materials Science, 46 (2001) 1-184.

[16] E. Ajayi, *Fabrication of Copper/Reinforced Carbon Nanotube Bipolar Plate Using Cold Spray*, 2016.

[17] J.E.B. Bickel, *Effect of annealing temperature on magnetocaloric properties and investigation of $Mn_xFe_{1.9-x}V_{0.02}P_{1-y}Si_y$ compounds*, Bachelor thesis, TU Delft, 2019.

[18] L. Zhang, O. Može, K. Prokeš, O. Tegus, E. Brück, *Neutron diffraction study of history dependence in MnFeP0.6Si0.4*, Journal of Magnetism and Magnetic Materials, 290-291 (2005) 679-681.

[19] X.F. Miao, *Magnetoelastic Coupling in Mn-Fe-P-Si Compounds*, Fundamental Aspects of Materials and Energy, TU Delft, 2016.

[20] P.J. Haines, M. Reading, F.W. Wilburn, *Chapter 5 - Differential Thermal Analysis and Differential Scanning Calorimetry*, in: M.E. Brown (ed.) Handbook of Thermal Analysis and Calorimetry, Vol. 1, Elsevier Science B.V., 1998, pp. 279-361.

[21] P. Roy, E. Brück, R.A. de Groot, *Latent heat of the first-order magnetic transition of $MnFeSi_{0.33}P_{0.66}$*, Physical Review B, 93 (2016).

[22] *Differential Scanning Calorimetry (DSC)* in, Vol. 2020, Technical Cell.

[23] M. McElfresh, *Fundamentals of magnetism and magnetic measurements*, Purdue University 1994.

[24] Hydrargyrum, *Bragg diffraction 2*, B.d. 2.svg (ed.), Wikipedia, 2011.

[25] S.T. Misture, R.L. Snyder, *X-ray Diffraction*, K.H.J. Buschow, R.W. Cahn, M.C. Flemings, B. Ilschner, E.J. Kramer, S. Mahajan, P. Veyssière (eds.) Encyclopedia of Materials: Science and Technology, Elsevier, Oxford, 2001, pp. 9799-9808.

[26] Z.Q. Ou, *Magnetic structure and phase formation of magnetocaloric Mn-Fe-P-X compounds*, Radiation, Radionuclides & Reactors, TU Delft, 2013.

[27] Z.Q. Ou, L. Zhang, N.H. Dung, L. Caron, E. Brück, *Structure, magnetism and magnetocalorics of Fe-rich $(Mn,Fe)_{1.95}P_{1-x}Si_x$ melt-spun ribbons*, Journal of Alloys and Compounds, 710 (2017) 446-451.

Appendix A

The *M* versus 1/*B* plots were fitted using the '*non-linear curve fitting*' of OriginPro 8.5 with the Boltzmann sigmoid function:

$$y = A_2 + \frac{(A_1 - A_2)}{1 + e^{\frac{x - x_0}{dx}}}$$

The fitting tool gave the following coefficients, errors and variances:

	A1		A2		x0		dx		Statistics	
	Value	SE	Value	SE	Value	SE	Value	SE	Red. χ2	Adj. R2
LP01	137.2904	0.07681	90.30838	1.76499	2.1041	0.03519	0.49137	0.01095	0.01531	0.99944
LP02	147.7878	0.18377	89.03219	1.23206	1.67158	0.01932	0.43577	0.01058	0.08888	0.99914
LP03	153.8681	0.09084	107.3504	0.66934	1.71543	0.01359	0.45573	0.00706	0.01876	0.99967
LP05	141.0936	0.2823	110.4102	0.81703	1.39604	0.02373	0.44723	0.02017	0.10375	0.9973
LP06	137.3517	0.30691	82.89281	1.45997	1.68099	0.03063	0.63569	0.0194	0.03192	0.99948
LP07	151.959	0.79567	95.17999	2.29927	1.58806	0.05105	0.85184	0.04608	0.03023	0.9994
LP08	150.6292	0.66278	83.59379	1.57493	1.43312	0.02442	0.70324	0.02557	0.05081	0.9995

Appendix B

The following table contains the XRD results after refinement of the nickel samples as well as those of the cobalt samples

Table 2: A table containing the XRD results obtained after Rietveld refinement of both the samples containing nickel and the samples containing cobalt.

Name	Composition	XRD							
		a, b	c	c/a	V	Main %	Imp. 3.1 %	Imp. 5.3 %	χ^2
AK10	$Mn_{0.62}Fe_{1.33}P_{0.66}Si_{0.34}$	6.01481	3.44019	0.57195	107.785	97.01	2.99	0.00	2.40
AK11	$Mn_{0.61}Fe_{1.33}Co_{0.01}P_{0.66}Si_{0.34}$	6.01082	3.44298	0.57280	107.729	95.80	4.20	0.00	2.05
LP01	$Mn_{0.61}Fe_{1.33}Ni_{0.01}P_{0.66}Si_{0.34}$	6.01050	3.44293	0.57279	107.716	96.77	3.23	0.00	2.90
AK12	$Mn_{0.60}Fe_{1.33}Co_{0.02}P_{0.66}Si_{0.34}$	6.00541	3.44570	0.57377	107.620	95.43	4.57	0.00	1.98
LP02	$Mn_{0.60}Fe_{1.33}Ni_{0.02}P_{0.66}Si_{0.34}$	6.00633	3.44508	0.57357	107.634	95.69	4.11	0.20	1.83
AK13	$Mn_{0.58}Fe_{1.33}Co_{0.04}P_{0.66}Si_{0.34}$	6.00470	3.44269	0.57333	107.501	95.66	4.34	0.00	1.78
LP03	$Mn_{0.58}Fe_{1.33}Ni_{0.04}P_{0.66}Si_{0.34}$	6.00006	3.44866	0.57472	107.521	96.30	3.95	0.16	1.74
AK14	$Mn_{0.56}Fe_{1.33}Co_{0.06}P_{0.66}Si_{0.34}$	6.00492	3.44465	0.57364	107.570	95.67	4.29	0.05	1.92
LP04	$Mn_{0.56}Fe_{1.33}Ni_{0.06}P_{0.66}Si_{0.34}$	5.99525	3.45004	0.57546	107.391	96.49	3.51	0.00	2.76
AK15	$Mn_{0.54}Fe_{1.33}Co_{0.08}P_{0.66}Si_{0.34}$	5.99862	3.44376	0.574093	107.316	96.24	3.76	0.00	1.83
LP05	$Mn_{0.54}Fe_{1.33}Ni_{0.08}P_{0.66}Si_{0.34}$	5.99187	3.44969	0.575728	107.259	95.62	3.53	0.31	2.22
AK16	$Mn_{0.52}Fe_{1.33}Co_{0.1}P_{0.66}Si_{0.34}$								
LP06	$Mn_{0.52}Fe_{1.33}Ni_{0.1}P_{0.66}Si_{0.34}$	5.98789	3.45129	0.576378	107.167	95.98	3.19	0.82	2.13
AK17	$Mn_{0.50}Fe_{1.33}Co_{0.12}P_{0.66}Si_{0.34}$	5.99341	3.43999	0.57396	107.013	97.12	2.88	0.00	1.98
LP07	$Mn_{0.50}Fe_{1.33}Ni_{0.12}P_{0.66}Si_{0.34}$	5.98258	3.45263	0.577114	107.018	96.40	3.62	0.00	2.01
LP08	$Mn_{0.48}Fe_{1.33}Ni_{0.14}P_{0.66}Si_{0.34}$	5.97831	3.45457	0.577851	106.926	95.94	3.65	0.42	1.74